Department Of Aerospace Engineering

Indian Institute Of Technology Madras

AS2070 : Aerospace Structural Mechanics

Snap-Through Buckling of Link-Arch Model

Members:
Hemant Meena (AE23B011)
V.Hari haran (AE23B031)
Adharsh Varma (AE23B045)
Mayank Kumar (AE23B051)
Smit Dhameliya (AE23B107)

Date: 02 May, 2025

Contents

List of Tables

List of Figures

1 Objectives

1. To observe and analyze the snap-through buckling phenomenon in a single degree-of-freedom (SDOF) link-arch model
2. To determine the relationship between the applied force and vertical displacement during snap-through buckling
3. To verify the theoretical predictions of equilibrium positions and critical loads

2 Apparatus

The experimental setup consists of the following components:

- **Base Platform:** Wooden block, 88 cm × 63 cm.
- **Aluminum Rods:** Two aluminium rods, working as a rails for the slider.(60 cm each).
- **Beams:** Two rigid beams, each approximately 22.5 cm in length.
- **Sliders:** Three rollers for the movement along the aluminium rods.
- **Springs:** Two steel springs (spring constant $K = 260\,\mathrm{N/m}$).
- **Force Gauge:** Spring gauge for accurate force measurements.

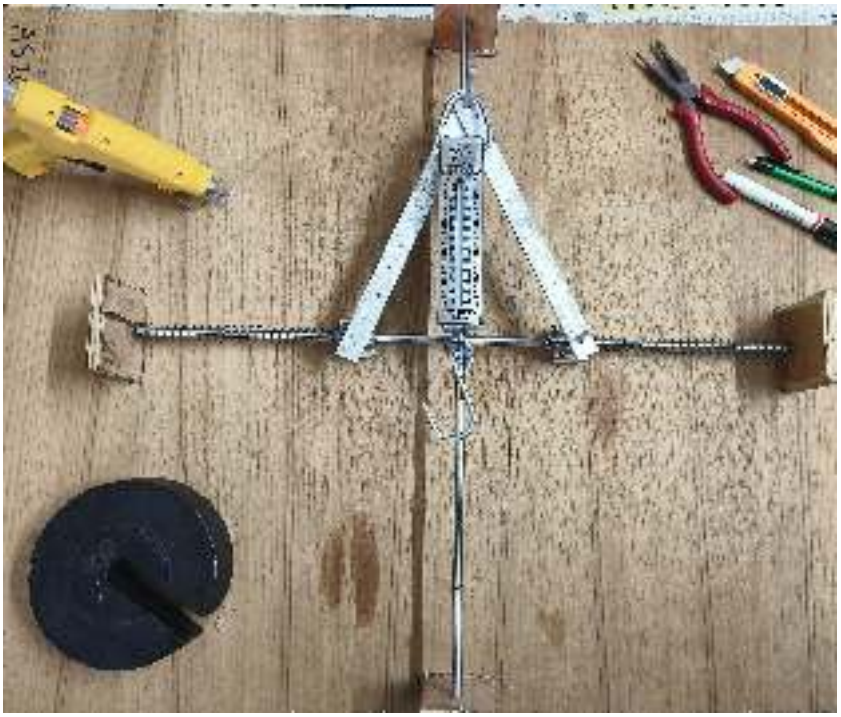

Figure 1: Experimental Apparatus

3 Theory

Snap-through buckling is a nonlinear instability phenomenon characterized by a sudden transition between equilibrium states when a critical load threshold is crossed. In the link arch model, this occurs through a limit point bifurcation where the system's tangent stiffness vanishes, enabling rapid configuration changes. The SDOF formulation provides fundamental insights into the essential mechanics while maintaining analytical tractability.

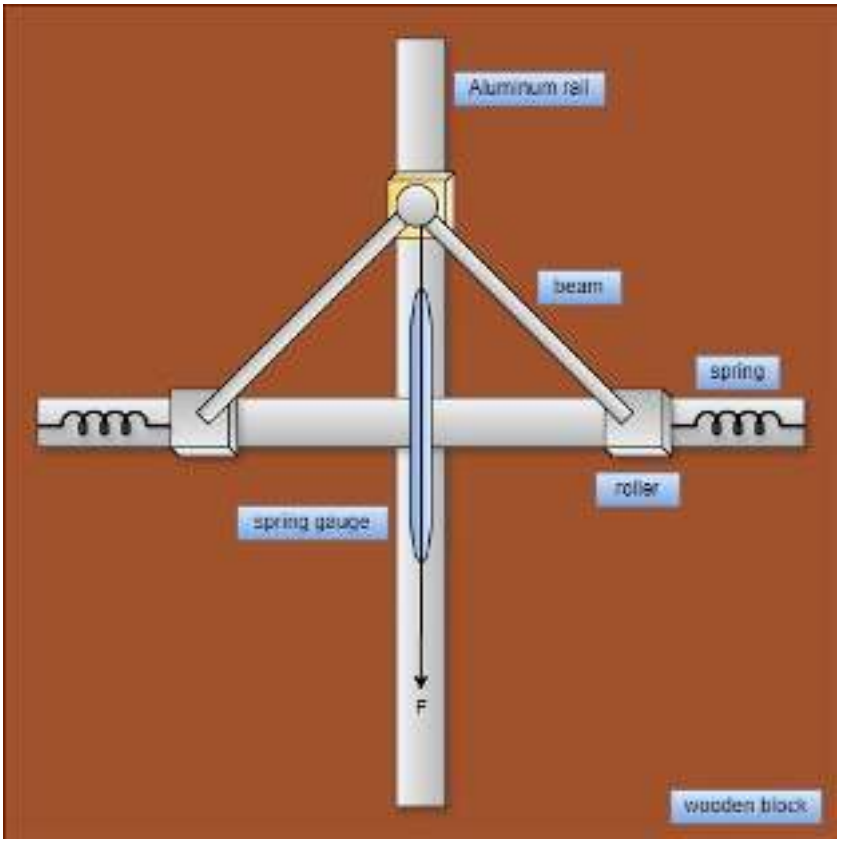

Figure 2: Schematic of Link Model Arch

3.1 Potential Energy Landscape

The system's behavior is governed by the potential energy function:

$$V(y) = k\left(\sqrt{L^2 - y^2} - \sqrt{L^2 - y_0^2}\right)^2 + Py \tag{1}$$

where the first term represents the strain energy stored in the lateral springs (incorporating nonlinear geometric stiffness), and the second term represents the work done by the vertical load P.

Equilibrium configurations satisfy $\frac{dV}{dy} = 0$, yielding:

$$P_{equil} = 2k\left(1 - \frac{\sqrt{L^2 - y_0^2}}{\sqrt{L^2 - y^2}}\right)y \tag{2}$$

This produces the characteristic S-shaped load-displacement curve shown in Figure 3, with three equilibrium branches for certain parameter ranges.

3.2 Stability Criteria

Stability is determined by the second derivative of the potential energy:

$$\frac{d^2V}{dy^2} = 2k\left[\frac{L^2 - y_0^2}{(L^2 - y^2)^{3/2}} - \frac{y^2}{L^2 - y^2}\right] - \frac{2ky}{\sqrt{L^2 - y^2}} \tag{3}$$

- **Positive values:** Stable equilibria (energy minima)
- **Negative values:** Unstable equilibria (energy maxima)

The limit points (snap-through thresholds) occur where $\frac{d^2V}{dy^2} = 0$, marking the transition between stable and unstable branches.

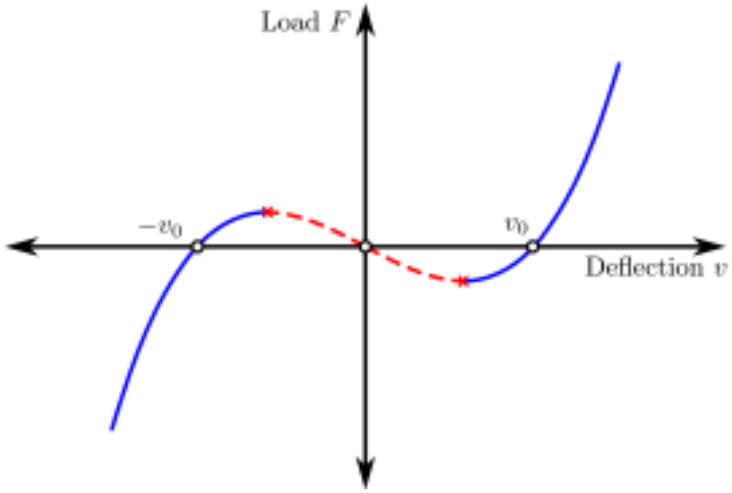

Figure 3: Applied Load vs Vertical Displacement Curve

3.3 Key Control Parameters

1. **Initial arch rise (y_0):** Higher y_0 increases the energy barrier between stable states but reduces the critical snap-through load. The dimensionless ratio y_0/L typically remains below 0.2 for shallow arches.

2. **Spring stiffness (k):** Stiffer springs raise both the peak load capacity and post-snap stiffness. Optimal designs balance snap-through sensitivity with load-bearing requirements.

3. **Loading rate:** Quasi-static loading produces deterministic snap-through at limit points, while dynamic loading can induce chaotic transitions between states through parametric excitation.

3.4 Design Implications

The link model captures essential features observed in real-world applications:

- **MEMS switches:** Snap-through provides digital switching action.
- **Aerospace panels:** Thermal buckling creates bistable configurations.

This formulation provides a foundation for analyzing more complex architectures while maintaining computational efficiency through its SDOF reduction.

4 Experimental Procedure

1. Fixed the 88 cm $\times$ 63 cm wooden base on a level surface
2. Mount parallel aluminum rods (60 cm each) 40 cm apart
3. Assemble the mechanism:
    - Connect two 22.5 cm beams with central hinge
    - Attach spring ends to beam tips ($k = 260$ N/m)
    - Install three sliders on aluminum rods
4. Attach spring gauge to central roller
5. Apply vertical force through central roller
6. Record force (spring gauge) vs position data
7. Continue loading until snap-through occurs
8. Reverse process by applying the force in opposite direction.

5 Calculations and Results

Given,

- Length of each rigid beam: L = 25 cm
- Initial height of the arch: $y_0 = 21.5$ cm
- The gravtational acceleration, g = 9.8 m/s^{-2}

5.1 Equations Used

The main equations used for analysis are:

- **Spring constant for helical compression spring:**

$$k = \frac{Gd^4}{8D^3n} \tag{4}$$

- **Number of coils (assuming close-coiled spring):**

$$n = \frac{L}{p} \tag{5}$$

- **Equilibrium force equation:**

$$P_{equil} = 2k\left(1 - \frac{\sqrt{L^2 - y_0^2}}{\sqrt{L^2 - y^2}}\right)y \tag{6}$$

- **Critical load determination:** The critical load corresponds to the maximum value of P on the force-displacement curve and can be found by solving:

$$\frac{dP}{dy} = 0 \tag{7}$$

5.2 Spring Constant Calculation

To determine the spring constant of a steel helical spring:

- Outer Diameter: $D_{outer} = 14$ mm
- Wire Diameter: $d = 1.2$ mm
- Pitch: $p = 4$ mm
- Length: $L = 150$ mm
- Shear Modulus for steel: $G = 79 \times 10^9$ Pa

Mean Coil Diameter:

$$D = D_{outer} - d = 14 - 1.2 = 12.8 \text{ mm} = 0.0128 \text{ m}$$

Number of Active Coils:

$$n = \frac{150}{4} = 37.5$$

Calculating spring constant:

$$k = \frac{79 \times 10^9 \times (0.0012)^4}{8 \times (0.0128)^3 \times 37.5}$$

$$k = \frac{0.1638}{6.29 \times 10^{-4}} \approx 260 \text{ N/m}$$

Final Result: The spring constant is approximately:

$$\boxed{k \approx 260 \text{ N/m}}$$

5.3 Sample Calculation

Given:

- Length of each rigid beam: $L = 22.5\,\text{cm} = 0.225\,\text{m}$
- Initial height of the arch: $y_0 = 21.5\,\text{cm} = 0.215\,\text{m}$
- Spring constant: $k = 260\,\text{N/m}$
- Gravitational acceleration: $g = 9.8\,\text{m/s}^2$

The potential energy of the system is given by:

$$V(y) = 260\left(\sqrt{0.051 - y^2} - 0.066\right)^2 + Py \tag{8}$$

The force-displaccement equation is:

$$P = 2k\left(1 - \frac{\sqrt{L^2 - y_0^2}}{\sqrt{L^2 - y^2}}\right) y$$

$$P = 520\left(1 - \frac{0.066}{\sqrt{0.051 - y^2}}\right) y$$

Sample calculation for $y = 16.5\,\mathbf{cm} = 0.165\,\mathbf{m}$:

$$\begin{aligned}
L^2 - y_0^2 &= 0.225^2 - 0.215^2 = 0.050625 - 0.046225 = 0.0044 \\
L^2 - y^2 &= 0.225^2 - 0.165^2 = 0.050625 - 0.027225 = 0.0234 \\
\sqrt{L^2 - y_0^2} &= \sqrt{0.0044} = 0.0663 \\
\sqrt{L^2 - y^2} &= \sqrt{0.0234} = 0.1529 \\
1 - \frac{\sqrt{L^2 - y_0^2}}{\sqrt{L^2 - y^2}} &= 1 - \frac{0.0663}{0.1529} = 1 - 0.4336 = 0.5664 \\
P_{\text{equil}} &= 2 \times 260 \times 0.5664 \times 0.165 \\
&= 520 \times 0.5664 \times 0.165 \\
&= 48.6\,\text{N}
\end{aligned}$$

Since the force is applied in the negative direction for positive displacement, we take:

$$P_{\text{equil}} = -48.6\,\text{N}$$

Percent Difference Calculation for $y = 16.5\,\mathbf{cm}$:
Given experimental applied force from Table 1 is $-98\,\text{N}$.

$$\begin{aligned}
\text{Percent Difference} &= \frac{|(-48.6) - (-98)|}{|-98|} \times 100\% \\
&= \frac{49.4}{98} \times 100\% \\
&= 50.4\%
\end{aligned}$$

5.4 Experimental and Theoretical Force-Displacement Data

Table 1: Experimental and Theoretical Force-Displacement Data

Disp. y (cm)	**Applied Force (N)**	**Theoretical Force (N)**	**Difference (%)**
16.5	-98	-48.6	50.4
10.0	-156.8	-34.9	77.7
7.5	-176.4	-26.8	84.8
-8	181.3	28.5	84.3
-9.5	156.8	33.3	78.7
-16	88.2	48.3	45.2

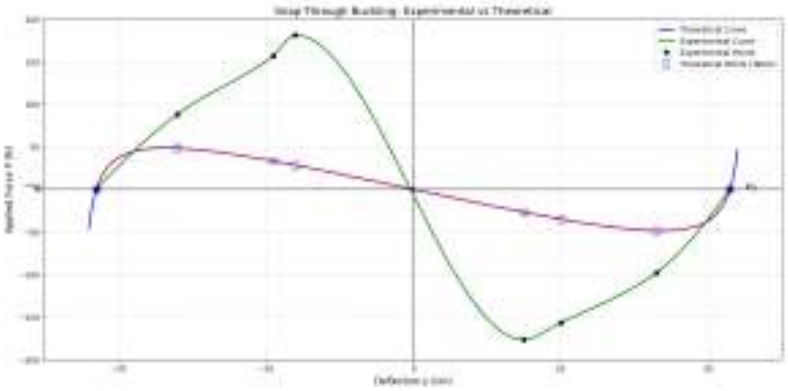

Figure 4: Theoretical and Experimental Curve

6 Source of error

- **Measurement Accuracy:** The spring gauge has limited precision, which could affect the accuracy of force measurements, especially at critical points like near the equilibrium points.
- **Friction Effects:** Despite using slider, there was friction in the system, due to absence of ball-bearings in sliders, affecting the horizontal movement of the beam ends and altering the force-displacement relationship.
- **Slider Mass Effects:** While assumed to be massless in the theoretical model, the actual slider used has some mass that may influence the dynamic behavior, especially during the snap-through transition.
- **Alignment Issues:** Misalignment of components, particularly the central hinge and end rollers, introduced the additional constraints for the model.
- **Data Acquisition Timing:** During snap-through, the displacement changes rapidly, making it challenging to capture the exact behavior with manual measurements.

7 Observation

1. The theoretical force values are calculated using the equilibrium force equation and applying the appropriate sign convention:
    - For positive displacements ($y > 0$), the force is negative.
    - For negative displacements ($y < 0$), the force is positive.

2. The large percent difference for some data points may indicate experimental errors or that the theoretical model does not perfectly capture real-world behavior near the initial position.

3. The percent differences suggest that while the model captures the general behavior of the system, there are significant quantitative discrepancies that could be due to friction, non-linear spring behavior, measurement errors, or simplifications in the theoretical model.

8 Conclusion

1. The experimental setup demonstrated bistability with two distinct equilibrium configurations (positive and negative displacements).

2. Significant discrepancies between experimental and theoretical forces were observed:

   - Largest difference: 84.8% at $y = 7.5\,\text{cm}$ (176.4 N vs 26.8 N)
   - Smallest difference: 45.2% at $y = -16\,\text{cm}$ (88.2 N vs 48.3 N)

   suggesting potential systematic errors in friction measurement or spring constant calibration.

3. Asymmetric behavior was observed in experimental forces, indicating possible misalignment in the experimental setup.

4. The force-displacement relationship followed theoretical trends qualitatively but not quantitatively:

   - Both experimental and theoretical forces increased with displacement magnitude
   - Experimental forces grew 3.6× faster (from 88.2 N at 16 cm to 181.3 N at 8 cm vs theoretical 48.3 N to 28.5 N)

5. The negative stiffness region (transition between stable states) showed unexpected hysteresis:

   - Required 98 N push force at $y = 16.5\,\text{cm}$ vs 88.2 N pull force at $y = -16\,\text{cm}$
   - Theoretical model predicted symmetric 48 N transition forces

6. Three key limitations were identified:

- Friction in pivot joints (unaccounted in theory)
- Assumption of massless beams and sliders vs actual mass of beams and sliders.
- Idealized pin supports vs real constrained rotations

7. Future improvements should:
    - Reducing the friction effects in the model
    - Use digital force sensors instead of manual weight stacking
    - Use of proper hinges at the joints.

9 Contribution

1. Hemant Meena : Experimental setup prepration and arranging the items.
2. V. Hari Haran : Contribute in Performing the experiment , ppt .
3. Adharsh Verma : Buying the items, Experimental contribution , ppt.
4. Mayank Kumar : Everything.
5. Smit Dhameliya : Everything except report and welding-drilling in the workshop.